Effects of Infill Walls on Load Resistance of Multi-Story RC Frames to Mitigate Progressive Collapse

Kai Qian[1,2]，Dong-Qiu Lan[1]，Shun-Kai Li[2], Feng Fu[2,3*]

[1]College of Civil Engineering and Architecture, Guangxi University, Nanning, China, 530004.

[2]College of Civil Engineering and Architecture at Guilin University of Technology, Guilin, China, 541004.

[3]School of Mathematics, Computer Science and Engineering, City, University of London, U.K.

ABSTRACT:

To study the effects of infill wall on progressive collapse resistance of reinforced concrete (RC) frames with slabs, a macro finite element (FE) model was built using general purpose software OpenSees. The FE model was validated by existing test results. Then, the model was subsequently used to predict the progressive collapse potential of eight-story RC frame including slabs and infill walls. The numerical studies demonstrated that the inclusion of the slabs and infill walls could increase the ultimate load and initial stiffness by 70% and 169%, respectively, compared with the bare frame. The infill walls not only changed the load resisting path but also effectively improved the load redistribution ability of the frame. To evaluate the reliability of using a two-story sub-structure to investigate the progressive collapse behavior of a multi-story building, the resistance of each story of a multi-story building in case of column missing is compared. It was found that the resistance of each story was similar, except the first story. Finally, a series of parameter studies were carried out to quantify the effects of opening ratio, thickness and compressive strength of the infill walls on the progressive collapse performance of RC frame.

* Corresponding author: E-mail address: feng.fu.1@city.ac.uk

Keywords: progressive collapse; infill wall; RC frame structure; numerical simulation

1. Introduction

Progressive collapse refers to the final damage zone is not proportional to the initial damage caused by accidental load. The occurrence of progressive collapse, such as the collapses of Ronan Point in 1968 and Word Trade Center in 2001, often leads to heavy casualties and huge property losses. The disastrous consequences of progressive collapse have brought great attention in structural engineering communities.

To deeply understand the load resisting mechanisms of RC frame under progressive collapse. A number of studies had been carried out based on Alternate Load Path (ALP) method. In the ALP method, one or several critical structural members, such as column, are removed notionally to simulate the initial damage. Then, concentrated load is applied on the top of the removed column to evaluate the ability of the remaining structure to bridge the initial damage. Yi et al. [1] conducted a quasi-static test of a 1/3 scale four-bay and three-story planar RC frame. It was found that the load resisting mechanisms such as flexural action and tensile catenary action (TCA) could be mobilized successively to resist progressive collapse. Su et al [2] and Yu and Tan [3] conducted experimental and analytical investigations on the progressive collapse behavior of beam-column sub-assemblages under middle column removal scenario. It was found that the effect of compressive arch action (CAA) increased with the decreased of span-depth ratio of the beam. The experimental results of Deng et al. [4] indicated that the use of high-strength concrete (HSC) could significantly enhance the CAA capacity, especially for the beams with low span-depth ratio. However, the high bond strength between the HSC and rebars may lead to premature fracture of the rebars, which hindered the further development of the TCA. Kim and Choi [5] conducted a test on five RC beam-column sub-

assemblages with and without strengthening. The test results indicated that the use of unbonded strands or side plates with stud bolts could greatly increase the progressive collapse resisting capacity of RC frames. For precast concrete (PC) beam-column structures, the CAA capacity and TCA capacity largely depended on joint detailing. Qian et al. [6-7] conducted static and dynamic tests on several series of PC beam-column sub-assemblages with high-performance dry connections. The failure modes and load resisting mechanisms of PC frames, which were different form conventional RC frames, were discussed. Yi et al. [8] conducted experimental studies on the performance of single-story RC flat plate structure following the loss of an interior column. It was found that compressive membrane action (CMA) and tensile membrane action (TMA) were the alternate load paths for the flat plate structure to mitigate progressive collapse. The effects of different strengthening methods on the collapse resistance of flat slab structures were experimental studied by Qian and Li [9-10]. In their works, a load distribution tree was designed to apply equivalent uniformly distributed load. Lu et al. [11] investigated the effects of beam height, slab thickness, and seismic details on RC beam-slab structures against progressive collapse. The contribution of CAA, TCA, CMA, and TMA for beam-slab substructures to resist progressive collapse was studied by Qian et al. [12-14]. Weng et al. [15] carried out numerical investigation on load redistribution capacity of multi-story flat slab substructures to resist progressive collapse. Gard et al. [16] numerically evaluated the effect of perimeter beams and shear walls on the static and dynamic response of flat slab structure to resist progressive collapse. The test results indicated that perimeter beams and shear walls can provide proper distribution of load path and hence reducing progressive collapse risks of flat slab structure.

In recent years, some researchers had paid attention to the effects of non-structural element,

such as infill walls, on the load resistance of RC frame against progressive collapse. Li et al. [17] experimentally and numerically investigated the effects of infill walls on RC frames to resist progressive collapse. Their study showed that the infill walls could remarkably increase the load resisting capacity and initial stiffness but reduce ductility of the frames. Qian and Li [18] tested three bare frames and corresponding infilled frames under the loss of a penultimate column scenario. The experimental results concluded that full-height solid infill walls could increase the first peak load and initial stiffness by 260% and 900%, respectively. Moreover, infill walls could help to reduce the shear deformation of the beam-column joints. Baghi et al. [19] demonstrated that masonry walls can increase the energy dissipation capacity and the toughness of the infilled frame 270% higher than bare frame. Brodsky and Yankelevsky [20] experimentally assessed the contribution of infill masonry walls to resist progressive collapse. It was concluded that the infill masonry wall can enhance vertical resistance of bare frame by around 280% on average and up to 500%. According to numerical studies [21-23], the use of masonry infill walls for multi-story building can considerably increase robustness. Furthermore, studies [24-28] proved that, even with openings, infill walls could greatly improve the performance of bare frames significantly.

As mentioned above, existing studies found that infill walls could improve the behavior of RC frames to resist progressive collapse even the infilled walls were punched. However, according the summary by Ibrahim et al. [29], most of the current research focused on two-dimensional (2D) sub-structures. In reality, the frames had RC slabs and transverse beams, which could increase the load resisting capacity significantly [14]. Thus, the enhancement efficiency of the infilled walls might be over-estimated based on 2D test models. Moreover, majority of existing studies on influence of infilled wall were just based on low-story frames. The effects of infilled walls on multi-story

buildings were still unclear. Thus, it was necessary to conducted studies on influences of infilled walls on three-dimensional (3D) multi-story buildings with transverse beams and RC slabs. In considering time and cost consumption, high computational FE software OpenSees was adopted for this numerical analysis. An 8-story RC frames was replicated after proper validation. Then, parametric studies were carried out to comprehensively understand the effects of infilled walls.

2. Numerical model and validation

2.1 Modeling details

In this study, the numerical models were built up by FE software OpenSees. Beams and columns were modeled using displacement-based nonlinear beam column elements (i.e., dispBeamColumn) with five Gauss-Legendre integration points along the element length. Infill walls were replicated by equivalent compressive struts, which were modeled using truss elements. T or L section was used to simulate the slab contribution. The effective flange width of each side was equal to four times of the slab thickness as suggested by Sasani [30]. Fiber division of these sections are shown in Fig. 1. The constitutive relationship of the materials was shown in Fig. 2. Steel02, a uniaxial Giuffre-Menegotto-Pinto steel material model with isotropic strain hardening was used to simulate reinforcement. Material MinMax was employed to define the failure strain of reinforcement. Concrete02 was employed to simulate the concrete material, which could consider the linear tensile performance of the concrete. Confinement was specified by the stress-strain relationships of Kent-Park model [31] modified by Scott et al. [32]. The concrete material concrete01 ignoring the tensile strength was employed to simulate the behavior of the equivalent compressive struts as tensile strength of infill walls was so low. According to Tsai and Huang [33-34], the compressive strut width of the wall panel a was determined as:

$$a = 0.175(\lambda l_b)^{-0.4} r_{\text{inf}} \tag{1}$$

$$\lambda = \left(\frac{E_m t_{\text{inf}} \sin 2\beta}{4 E_{fe} I_b l_{\text{inf}}}\right)^{0.25} \tag{2}$$

where r_{inf} is the diagonal length of the infill panel; I_{b} is moment of inertia of beam; E_{fe} is elastic modulus of frame and is determined to $5000\sqrt{f_c}$ [35], f_c is the compressive strength of concrete; t_{inf} is thickness of infill panel and equivalent strut; l_{inf} and h_{inf} are length and height of infill panel, respectively; β is the angle of strut, $\beta = \arctan(\frac{l_{\text{inf}}}{h_{\text{inf}}})$; E_m is elastic modulus of infill wall, $E_{\text{m}} = 550 f_m$ [36], f_m is the compressive strength of infill wall.

To simulate the interaction between infill wall and frame, single-strut model [37], double-strut model [38] and triple-strut model [39] were all used and compared. The layout of single-strut, double-strut, and triple-strut model were shown in Figs. 3(a), (b) and (c), respectively. It should be noted that, equivalent struts actually were applied in both two diagonal directions, but only the strut in one of the directions was illustrated herein. As shown in the Fig. 3(b), the contact length of the double struts was calculated as $z/3$ [40], and z was determined by $\pi/(2\lambda)$ [41]. According to El-Dakhakhni et al. [39], the contact length of the struts on the beam ($\alpha_b l_b$) and column ($\alpha_{col} h_{col}$) of the triple-strut model were suggested as Eqs. (3) and (4), respectively.

$$\alpha_b l_b = \left[\frac{2(M_{pj} + \beta_b M_{pb})}{f_{m-90} t_{\text{inf}}}\right]^{0.5} \le 0.4 l_b \tag{4}$$

$$\alpha_{col} h_{col} = \left[\frac{2(M_{pj} + \beta_{col} M_{pcol})}{f_{m-0} t_{\text{inf}}}\right]^{0.5} \le 0.4 h_{col} \tag{5}$$

where α_b is the ratio of beam contact length to the span of beam; α_{col} is the ratio of column contact length to the height of column; M_{pb} and M_{pc} are the beam and column plastic moment capacities, respectively; M_{pj} is the minimum of M_{pb} or M_{pc}; β_b and β_{col} are the bending moment reduction

128 factor of the beam and column, both of them taking 0.2; f_{m-90} is infill wall compressive strength
129 perpendicular to bed joints, $f_{m-90} = f_m$, f_{m-0} is infill wall compressive strength parallel to bed joints,
130 $f_{m-0} = 0.7 f_m$ [42].

131 For the frame with partial infill walls, infill walls around the openings should be divided into
132 independent region and each region was modeled by a pair of diagonal equivalent compressive struts,
133 the width of which was calculated by Eqs. (1) and (2) [25], [43-44]. It should be noted that, the
134 effective struts width of infill region w is assumed as $a/2$, because the frame members
135 constraining only one side of diagonal region [25], [43]. For example, as shown in Fig. 4, a
136 perforated infill wall of Specimen WF-L would be introduced in follow Section 2.2, which can be
137 divided in to four regions, and replaced by strut 1, 2, 3 and 4, respectively. For the macro model for
138 WF-L, w is 61 mm for strut 1, 1'and 3, 3', 56 mm for strut 2, 2', 79 mm for strut 4, 4' as shown in
139 Fig. 4.

140 2.2 Model validation

141 To validate the reliability of numerical models, experimental results presented by authors'
142 published paper [28] were utilized for comparison. As presented in Qian et al. [28], a series of five
143 1/4 scaled RC frames with and without infill walls were tested to assess the progressive collapse
144 resistance under the scenario of loss of a penultimate column. Specimen WF with solid infill walls
145 and Specimen WF-L with punched infilled walls were carried out. The geometry and reinforcement
146 details of WF-L was shown in Fig. 5. Specimens WF and WF-L have identical RC frame but different
147 infill walls. The concrete cylinder compressive strengths of WF and WF-L measured on the day of
148 testing were 34 MPa and 32 MPa, respectively. The measured compressive strength and shear
149 strength of masonry unit were 10.5 MPa and 1.1 MPa, respectively. The properties of reinforcements
150 were shown in Table 1. Regarding more detailed results, please refer to Qian et al. [28]. For WF, the

compressive strut width a for single-strut was calculated as 157 mm. The contact length of the struts $\alpha_b l_b$ and $\alpha_{col} h_{col}$ for triple-strut model were calculated as 87 mm and 122 mm, respectively. Comparison of load-displacement curves from tests and numerical models, as shown in Fig. 6(a). The first peak load obtained from single-strut, double-strut, and triple-strut models are 128 kN, 107 kN, and 135 kN, respectively. Thus, the errors of the first peak load from the single-strut, double-strut, triple-strut models were 12%, 6% and 18%, respectively. As shown in the figure, all three models were able to simulate the interaction between the infill wall and the surrounding frame well, especially the single-strut and double-strut model could accurately reflect the general characteristic of the load-displacement curve. Thus, single-strut model was utilized for simulation of WF-L and following parametric studies. As shown in Fig. 6(b), the numerical simulations with single-strut model agreed with the test results of WF-L well.

To evaluate the reliability of numerical models for 3D frames with or without slabs, experimental results (T1 and S1) presented by authors' another paper [14] were utilized for validation. As shown in Fig. 7, T1 is a crisscross frame with five columns, four beams. The dimensions of the columns were 200 × 200 mm, which was enlarged for preventing damage in the columns. The center-to-center spans of the transverse and longitudinal beams were 1,500 and 2,100 mm, respectively. Moreover, the cross-sectional dimensions of transverse and longitudinal beams were 140 × 80 mm and 180 × 100 mm, respectively. S1 is a 2×2 bay single-story beam-slab sub-structure, including nine columns, twelve beams, and a 55 mm RC slab. The cross-sectional dimension of beams and columns of Specimen S1 are identical to Specimen T1. The measured cylinder compressive strengths of concrete were 21.5 MPa and 21.4 MPa for T1 and S1, respectively. The properties of reinforcements were shown in Table 1.

Comparison of the load-displacement curve of T1, as shown in Fig. 8(a), indicated that the numerical model could reflect the development of CAA and TCA well. The first peak load obtained from experimental and numerical result was 67 kN and 66 kN, respectively. For S1, as shown in Fig. 8 (b), the numerical model could predict the first peak load, ultimate load, and ultimate displacement well. The first peak load and ultimate load obtained from test were 115 kN and 169 kN, respectively. However, that from numerical results were 114 kN and 170 kN, respectively. Based on these validation, multi-story 3D frames including slab components were built up.

3. Extended studies

3.1 A multi-story 3-D frame model

As shown in Fig. 9, an 8-story building was designed in accordance with ACI 318-14 (2014) [45], [46-49]. The building has span length of 6000 mm in Y-direction and 4200 mm in X-direction, story height of the first story and upper stories are 3600 mm and 3300 mm, respectively. The design live load is 2.0 kN/m^2 and the dead load including self-weight is 6.4 kN/m^2. The cross-section of column is 550 mm×550 mm. The cross-section of beams in the X and Y direction are 500 mm×300 mm and 550 mm×300 mm, respectively. The thickness of slab is 120 mm. Fig 9(c) illustrates the reinforcement details of the beams, columns, and slabs. The cylinder compressive strength of concrete was assumed to be 24 MPa. The yield strength and ultimate strength of longitudinal reinforcement was assumed as 400 MPa and 540 MPa respectively. The compressive strength of masonry unit was 3.8 MPa.

To quantify the effects of infill walls and slabs on load resisting capacity of multi-story RC frames, FE models of bare frame (BF), bare frame with slabs (SF1), infilled frame (WF1) without slabs and infilled frame with slabs (SWF1) were built accordingly. For the infilled frame, except the

first story, all the upper stories contained infill walls. Fig. 10 shows the overall configuration of the model of 8-story of infilled frame. As shown in the figure, each infill wall panel was replaced by a pair of equivalent struts. Then, quasi-static analyses for these models subjected to the loss of a middle column in X-direction (hereinafter referred to as "middle column") were carried out.

3.2 Overall load resistance of the frame

To quantify the load resistance contribution of the slab and infill wall to resist progressive collapse, the load resistance of infilled frames was quantified by subtracting the load resistance of frames with slab and infilled frames by that of bare frame at the critical displacement. As shows in Fig. 11, the first peak load of BF1 was obtained as 4596 kN at a displacement of 85 mm. Beyond this point, load resisting capacity began to drop due to concrete crushing. When the displacement further increased to 720 mm, the TCA capacity of 4100 kN was obtained. As shown in Table 2, the initial stiffness of Model BF1 was 267×10^3 kN/m. For Model SF1, the initial stiffness was 360×10^3 kN/m, which was 35% higher than that of BF1. When the displacement reached 88 mm, the first peak load of 5923 kN was achieved, which was 129% of that of BF1. The load resistance re-ascending was observed when the displacement reached 570 mm due to the development of TCA and TMA. The ultimate load capacity of SF1 was measured to be 4956 kN at a displacement of 650 mm. Beyond this point, the resisting load capacity dropped sharply to 4482 kN because of fracture of the longitudinal reinforcement. For infilled frame WF1, the initial stiffness of 665×10^3 kN/m, which was 249% of that of BF1. When the displacement reached 27 mm, the first peak load of 6881 kN, which is 150% of BF1, was measured. When the displacement increased to 712 mm, the load capacity of TCA reached 4595 kN, which was 67% of the first peak load. For Model SWF1, considering both effects of slab and infill wall, the initial stiffness was 717×10^3 kN/m, which was 268% of that of BF1. The first peak load of 7812 kN was obtained at a displacement of 29 mm,

which was 170% of that of BF1. At a displacement of 648 mm, the load capacity of TCA was 5361 kN, which is 69% of the first peak load.

The comparison of load-displacement indicated that ignoring the effects of slabs and infilled walls was very conservative when evaluating the load resisting capacity of RC structures to mitigate progressive collapse, as shown in Fig.11. Moreover, evaluation of the efficiency of infill walls based on 2D model, which ignored the slab contribution, may over-estimate the efficiency.

3.3 Axial force in beams

Fig. 12 shows the variation of axial force of the beams in the first, fourth, and eighth story above the removed column. In X-direction, only the axial force of the beam on the right side of the removed column is presented due to symmetric. For the beam of BF1 and SF1 in X direction, compressive axial force was observed initially, which implicitly reflected the development of the CAA. It was seen that the compressive force in the beam of the first story was largest, this could be attributed to the strongest boundary condition of the first story. For the same reason, the greatest tensile axial force was also developed in the beam on first story. Different from BF1 and SF1, the beams of infilled structures WF1 and SWF1 in X direction experienced tensile axial force first. This is because the infill wall transferred majority of the load by the equivalent compressive struts. The equivalent compressive struts prone to push the side joints outward. As a result, tensile force was developed in the beams in X direction. With the increase of displacement, the axial force of the beams in the X direction of WF1 and SWF1 exhibited similar trend to BF1 and SF1. Regarding the beam in Y direction, it was found that the first story beam of the structures without slab experienced compressive axial force during the collapse process, whereas the axial force developed in the beams in other stories was tensile. Additionally, it was found that the higher the story, the larger the axial force. The axial forces in the beams of SF1 and SWF1 were much greater than the ones in BF and

WF1, as the beams of SF1 and SWF1 included flanges provided larger tensile force at large deformation stage. Therefore, the influence induced by the infill walls on the development of the beam axial force was mainly reflected at the initial loading stage, but had little effect on the subsequent loading history.

3.4 Load resistance at each story

Figs. 13 (a) and (b) illustrate the load resistance of each story in model BF1 and SWF1, respectively. For BF1, it was found that the load resistance of each story was almost the same except the first story. At the initial loading stage, the first peak load of the first story was higher than other stories because the first story had the strongest boundary condition. As shown in Fig. 14, the joints of the first story experienced the smallest horizontal outward movement, which implicitly indicated that the first story had the strongest boundary constraints. However, the resistance of the first story is close to other story with the increase of displacement. Differently, the first story of SWF1 had the lowest resistance as no infill wall was built in this story. The eighth story had the second lowest resistance due to relatively lower boundary condition. However, the second to seventh story achieved similar resistance. In summary, the different between the resistance of each story could be attributed to the different boundary condition.

3.5 Load redistribution

Generally, the corner column had highest vulnerability for terrorist attack and vehicular impact [50-53]. Thus, it was necessary to evaluate the effects of infill walls on the structures subjected to the loss of a corner column removal. As shown in Fig. 15, the suffixes "-M" and "-C" distinguished the loss of the Middle column and Corner column, respectively. For SF1-C, the first peak load and the initial stiffness were 3307 kN and 163×10^3 kN/m, respectively, which were only 56% and 45% of that of SF1-M, respectively. In comparison, the first peak load and initial stiffness of SWF1-C

were 4793 kN and 359×10^3 kN/m, which were 45% and 120% higher than those of SF1-C, respectively.

When a building experiences a column suddenly removed, the axial force initially sustained by the removed column would be redistributed to adjacent columns. To study the load redistribution behavior of the frames with and without infill walls, the reaction force of the adjacent columns was outputted. Figs. 16(a) and (b) respectively illustrate the load redistribution ratio of Model SF1and SWF1 at the stage of first peak load. For Model BF1, as shown in Fig. 16 (a), after the removal of middle column (column A-4), approximately 34%, 34% and 24% of the axial force was redistributed to the adjacent columns A-3, A-5 and B-4, respectively, while the load redistribution ratios of other columns were so small to be ignored. For model SWF1, similar to SF1, most of the load was redistributed into the adjacent columns A-3, A-5 and B-4. However, their load redistribution ratios were decreased, indicating that the infill wall successfully transferred the redistributed load to other columns, especially those in plane of the infill walls.

Fig. 17 (a) shows the load redistribution ratios of each column after removing the corner column (A-1 column) of SF1. As shown in the figure, at the stage of first peak load, 61% and 45% of the load were redistributed into Column A-2 and Column B-1, respectively. Due to the relatively single load transfer path, only 3% and 0% of the axial force were redistributed into Columns A-3 and C-1, respectively. As shown in Fig. 17(b), after the conner column of SWF1 has been removed, 49% and 39% of the load were redistributed to Column A-2 and Column B-1, respectively. Compared to SF1, more load was redistributed into Column A-2 and Column B-1. Therefore, the enhancement effectiveness of the infill wall was greater in the scenario of a corner column loss.

3.6 Dynamic progressive collapse resistance

In this study, nonlinear static analysis was used. However, the dynamic effect should be

287 considered due to the nonlinear dynamic nature of progressive collapse. Energy-based method is one
288 of the most widely used methods to transfer the static resistance to dynamic resistance [54-55].
289 According to the framework proposed by Izzuddin et al. [56] shown in follows

290 $$P_{\mathrm{d}}(u_d) = \frac{1}{u_d}\int_0^{u_d} P_{NS}(u)du \tag{6}$$

291 where $P_{\mathrm{d}}(u)$ and $P_{NS}(u)$ are the dynamic progressive collapse resistance and static progressive
292 collapse resistance estimated at the displacement demand *u*, respectively.

293 As shows in Fig. 18, the dynamic resistance of models BF1, SF1, WF1, and SWF1 were
294 determined as 4232 kN, 5311 kN, 5629 kN, and 6524 kN, respectively. Therefore, when dynamic
295 effect was considered, the load resistance of models SF1, WF1, and SWF1 were increased by 25%,
296 33%, and 54% compared with BF.

297 **4. Parametric studies**

298 4.1 Effects of opening ratios

299 To study the effects of opening ratios of infill wall on the load resistance, 8-story frames with
300 21%, 32%, 42% and 53% opening ratio in the infill wall were modeled and compared with the frame
301 with solid walls. Schematic diagrams of opening layout of the infill wall in different models are
302 shown in Fig. 19. The load-displacement curves and normalized first peak load of the models with
303 different opening ratios are shown in Figs. 20 and 21, respectively. With the opening ratio of 21%,
304 32%, 42%, and 53%, the infilled frames obtained the first peak load of 7581 kN, 7241 kN, 6818 kN,
305 and 6275 kN, respectively, which was 3%, 7%, 13%, and 20% lower than that of the model with
306 solid wall SWF1. This indicated that even the opening ratio achieved 53%, the decrease of the first
307 peak load was only 20 %. Thus, it was over-conservative to ignore the effects of infill walls when
308 opening existed.

309 4.2 Effects of number of stories

310 Based on Model SF1, a series of 2-story, 4-story, and 6-story bare frames with slab were built,
311 which were collectively called as SF series. Similarly, the SWF series considering both of slab and
312 infill wall were built by referring to Model SWF1. It should be noted that, expect the first story, all
313 the upper stories contain infill walls. As shown in Fig. 22, for the SF series, the first peak load of 2-
314 story, 4-story, 6-story, and 8-story frames were 1517 kN, 2988 kN, 4455 kN and 5923 kN,
315 respectively, which increased proportionally. For the SWF series, the first peak load of 2-story, 4-
316 story, 6-story, and 8-story frames were 1930 kN, 3791 kN, 5856 kN, and 7812 kN, respectively. Thus,
317 the first peak load of 4-story, 6-story, and 8-story frames was 2 times, 3 times and 4 times of that of
318 2-story frame, respectively. Moreover, the first peak load of SWF series frames was approximate 1.3
319 times of that of SF series with the same number of stories. Thus, the story number may not affect the
320 enhancement efficiency of the infill walls and slabs.

321 4.3 Effects of thickness of infill walls

322 The effect of variation in the thickness of infill walls on the resistance of the infilled frame
323 SWF1 is presented in Fig. 23. According to Eqs. (1) and (2), the equivalent diagonal compressive
324 struts width would change with the variation of the thickness of infill walls, as shown in Table 3. For
325 the infilled frame with infill thickness of 0.4, 0.6, 0.8, 1.0 and 1.2 times of the designed thickness
326 (190mm), the corresponding first peak load was 6179 kN, 6715 kN, 7274 kN, 7812 kN, and 8414
327 kN, respectively. When the thickness increased by 0.2 times of the designed thickness, the first peak
328 load can increase by 7% - 9%, showing a linear growth. As shown in Table 3, the increase of the
329 thickness can significantly increase the structural initial stiffness.

330 4.4 Effects of compressive strength of infill walls

331 The effects of variation in the compressive strength of infill walls on the structural resistance
332 is illustrated in Fig. 24. As shown in the figure, for the infilled frame with the compressive strength

of infill panel of 0.25, 0.5, 0.75, 1.0 and 1.25 times of the designed value of 3.8 MPa, the corresponding first peak load was 6004 kN, 6438 kN, 7129 kN, 7812 kN, and 8554 kN, respectively. When the compressive strength of infill wall was increased by 0.25 times of 3.8 MPa from 1.9 MPa to 4.75 MPa, the first peak load can increase by 7% to 11%. Compare to the frame without infill wall (SF1), compressive strength of 0.25 times of 3.8 MPa only increase the first peak load by only 1%, which can be ignored.

5. Conclusions

In this paper, macro FE models were utilized to study the effects of infill walls on progressive collapse resistance of multi-story RC frames. After validation, a series of 8-story frames were built and compared to quantify the resistance contribution of slab and infilled wall. In addition, extended studies were carried out to investigate the effect of infill walls on load resistance at each story and load redistribution behavior of the frames. A series of parameters studies on opening ratios, number of stories, thickness and compressive strength of the infill walls were carried out. The main conclusions of this study are as follows：

1. The numerical model could simulate the effects of infill walls and slabs well. Although tripe-strut model for infill wall simulation could predict the load-displacement curve of test results best, the accuracy of single-strut model is acceptable. Moreover, numerical results indicated that using T-shape and L-shape section with beam flange width of 4 times of slab thickness in each side was able to reflect the effect of the slab well.
2. Based on solid validation, a full-scale 8-story 3D frame model was built up for evaluation the influence of infill walls and RC slabs in realistic situation. It was found that the infill wall could increase the initial stiffness and the first peak load of the planar frames up by 149% and 50%,

355 respectively. For 3D frames with slabs, the infill wall increased the initial stiffness and the first
356 peak load by 99% and 32%, respectively. Thus, the enhancement efficiency of the infill wall
357 was reduced when RC slab and transverse beams were included in the models. However,
358 ignoring the effects of infill walls was over-conservative even the infill walls have opening ratio
359 as large as 53%. It was found that the RC slab could increase the first peak load of the multi-
360 story frame by 29% and 23%, when infill walls were excluded and included, respectively.
361 3. According to the discussion on the beam axial force, it was found that the infill wall transferred
362 majority of the load initially but had little effects on the load resistance at large deformation
363 stage. Based on the load redistribution results of the infilled frame, it was found that, due to
364 exist of the infill wall, the load initially resisted by the removed column was more uniformly
365 redistributed to surrounding columns.
366 4. For bare frames, the beams in the first story had greatest compressive arch action and tensile
367 catenary action due to strongest horizontal boundary constraints. It was found that the story
368 number may not affect the enhancement efficiency of the infill walls and slabs. The thickness
369 and compressive strength of infill walls may affect the enhancement efficiency of infill walls
370 significantly. However, when the compressive strength as low as 0.95 MPa, the influence of
371 infill walls could be ignored.
372

373 **Acknowledgements**

374 The authors gratefully acknowledge the financial support provided by the Natural Science
375 Foundation of China (Nos. 52022024，51778153). Any opinions, findings and conclusions expressed
376 in this paper do not necessary reflect the view of Natural Science Foundation of China.

References

[1] Yi WJ, He QF, Xiao Y. Experimental study on progressive collapse-resistant behavior of reinforced concrete frame structures. ACI Struct J 2008; 105(4): 433-439.

[2] Su YP, Tian Y, Song XS. Progressive collapse resistance of axially-restrained frame beams. ACI Struct J 2009; 106(5): 600-7.

[3] Yu J, Tan KH. Structural behavior of RC beam-column subassemblages under a middle column removal scenario. J Struct Eng 2013; 139: 233-250.

[4] Deng XF, Liang SL, Fu F, Qian K. Effects of high-strength concrete on progressive collapse resistance of reinforced concrete frame, J Struct Eng 2020; 146(6): 04020078.

[5] Kim J, Choi H. The monotonic loading tests of RC beam-column subassemblage strengthened to prevent progressive collapse, Int J Concr Struct Mater 2016; 9(4):401–13.

[6] Qian K, Liang SL, Fu F, Fang Q. Progressive collapse resistance of precast concrete beam-column sub-assemblages with high-performance dry connections. Eng Struct 2019; 198: 109552.

[7] Qian K, Liang SL, Xiong XY, Fu F, Fang Q. Quasi-static and dynamic behavior of precast concrete frames with high performance dry connections subjected to loss of a penultimate column scenario. Eng Struct 2020; 205: 110115.

[8] Yi WJ, Zhang FZ, Kunnath SK. Progressive collapse performance of RC flat plate frame structures. J Struct Eng 2014; 140(9): 04014048.

[9] Qian K, Li B. Load-resisting mechanism to mitigate progressive collapse of flat slab structures. Mag Concr Res 2015; 67(7): 349–363.

[10] Qian K, Li B. Strengthening of multibay reinforced concrete flat slabs to mitigate progressive collapse. J Struct Eng 2015; 141: 04014154.

[11] Lu XZ, Lin KQ, Li Y, Guan H, Ren PQ, Zhou YL. Experimental investigation of RC beam-slab substructures against progressive collapse subject to an edge-column-removal scenario, Eng Struct 2017; 149: 91–103.

[12] Qian K, Li B. Slab Effects on response of reinforced concrete substructures after loss of corner column. ACI Struct J 2012;109(6): 846-855.

[13] Qian K, Li B, Zhang ZW. Testing and simulation of 3D effects on progressive collapse resistance of RC buildings. Mag Concr Res 2015; 67(4): 163–178.

406 [14] Qian K, Li B, Ma J X. Load-carrying mechanism to resist progressive collapse of RC buildings.
407 J Struct Eng 2015; 141(2): 4014107-1.
408 [15] Weng YH, Qian K, Fu F, Fang Q. Numerical investigation on load redistribution capacity of flat
409 slab substructures to resist progressive collapse. J Build Eng 2020; 29, pp. 101109–101109.
410 [16] Garg S, Agrawal V, Nagar R. Case study on strengthening methods for progressive collapse resistance of RC
411 flat slab buildings. Struct 2021; 28: 1709–1722.
412 [17] Li S, Shan SD, Zhai CH, Xie LL. Experimental and numerical study on progressive collapse
413 process of RC frames with full-height infill walls, Eng Fail Anal 2016; 59: 57-68.
414 [18] Qian K, Li B. Effects of masonry infill wall on the performance of RC frames to resist
415 progressive collapse. J Struct Eng 2017; 143(9): 04017118.
416 [19] Baghi H, Oliveira A, Valença J, Cavaco E, Neves L, Júlio E. Behavior of reinforced concrete
417 frame with masonry infill wall subjected to vertical load. Eng Struct 2018;171(15):476–87.
418 [20] Brodsky A, Yankelevsky DZ. Resistance of reinforced concrete frames with masonry infill walls
419 to in-plane gravity loading due to loss of a supporting column. Eng Struct 2017; 140:134–50.
420 [21] Xavier FB, Macorini L, Izzuddin BA. Robustness of multistory buildings with masonry infill. J
421 Perform. Constr Facil 2015; B4014004.
422 [22] Xavier FB. The role of masonry infill in progressive collapse mitigation of multi-storey
423 buildings. PhD dissertation, Imperial College London, London; 2015.
424 [23] Barrosa M, Cavacob E, Nevesc L, Júliod E. Effect of non-structural masonry brick infill walls
425 on the robustness of a RC framed building severely damaged due to a landslide. Eng Struc. 2019;
426 180(1):274-83.
427 [24] Tsai MH, Huang TC. Progressive collapse analysis of an RC building with exterior partially
428 infilled walls. Struct Design Tall Spec Build 2013; 22:327–348.
429 [25] Shan SD, Li S, Xu SY, Xie LL. Experimental study on the progressive collapse performance of
430 RC frames with infill walls. Eng Struct 2016, 111: 80-92.
431 [26] Shan SD, Li S, Kose MM, Sezen H, Wang SH. Effect of partial infill walls on collapse behavior
432 of reinforced concrete frames. Eng Struct 2019; 197:109377.
433 [27] Yu J, Gan YP, Wu J, Wu H. Effect of concrete masonry infill walls on progressive collapse
434 performance of reinforced concrete infilled frames. Eng Struct 2019; 191:179-193.
435 [28] Qian K, Lan DQ, Fu F, Li B. Effects of infilled wall opening on load resisting capacity of RC

436 frames to mitigate progressive collapse risk. Eng Struct 2020, 223:111196.
437 [29] Alshaikh IMH, Bakar BHA, Alwesabi EA.H., Akil HM. Experimental investigation of the
438 progressive collapse of reinforced concrete structures: An overview. Struct 2020; 25: 881–900
439 [30] Sasani M. Response of a reinforced concrete infilled-frame structure to removal of two adjacent
440 columns. Eng Struct 2008; 30: 2478–2491
441 [31] Kent DC, Park R. Stress-strain behavior of concrete confined by overlapping hoops at low and
442 high strain rates, J Struct Div 1971; 97 (7): 1969-1990.
443 [32] Scott BD, Park R, Priestley MJN. Stress-strain behavior of concrete confined by overlapping
444 hoops at low and high strain rates. ACI J 1982; 79(1): 13-27.
445 [33] Tsai MH, Huang TC. Effect of interior brick-infill partitions on the progressive collapse
446 potential of a RC building: linear static analysis results. Int J Eng Appl 2010; 6(1):1–7.
447 [34] Tsai MH, Huang TC. Numerical investigation on the progressive collapse resistance of an RC
448 building with brick infills under column loss. Int J Civil and Environ Eng 2011; 5(10): 483–90.
449 [35] Park R, Paulay T. Reinforced concrete structures. Wiley, New York, 769 pp; 1975.
450 [36] FEMA (Federal Emergency Management Agency). Prestandard and commentary for the seismic
451 rehabilitation of buildings. FEMA 356, Washington, DC, 2000.
452 [37] MSJC (Masonry Standards Joint Committee). Building code requirements for masonry
453 structures. Reston, VA: ASCE, 2011.
454 [38] Crisafulli FJ. Seismic behaviour of reinforced concrete structures with masonry infills. PhD
455 Thesis. University of Canterbury, New Zealand. 1997.
456 [39] El-Dakhakhni WW, Elgaaly M, Hamid AA. Three-strut model for concrete masonry-infilled
457 steel frames. J Struct Eng 2003; 129:177-185.
458 [40] Uva G, Raffaele D, Porco F, Fiore A. On the role of equivalent strut models in the seismic
459 assessment of infilled RC buildings. Eng Struct 2012; 42: 83–94.
460 [41] Stafford SB. Behaviour of square infilled frames. Journal of Structural Division 1966;
461 92(1):381–403.
462 [42] Dawe JL, Swah CK. Analysis of concrete masonry infilled steel frames subjected to in-plane
463 loads. Proceeding of the 5th Canadian Masonry Symposium. Vancouver, British Columbia, 1989;
464 329-340.
465 [43] Nyunn S, Wang F, Yang J, Liu QF, Azim I, Bhatta S. Numerical studies on the progressive

collapse resistance of multi-story RC buildings with and without exterior masonry walls. Struct 2020; 28:1050-1059.

[44] Shan SD, Li S. Fire-induced progressive collapse mechanisms of steel frames with partial infill walls. Struct 2020; 25: 347–359.

[45] ACI Committee 318. Building code requirements for structural concrete (ACI 318-14) and commentary. American Concrete Institute, Farmington Hills, MI; 2014.

[46] Fu F. Progressive collapse analysis of high-rise building with 3-D finite element modeling method. Journal of Constructional Steel Research 2009; 65(6), pp. 1269–1278

[47] Fu, F. Response of a multi-storey steel composite building with concentric bracing under consecutive column removal scenarios. Journal of Constructional Steel Research 2012; 70, pp. 115–126.

[48] Fu, F. 3-D nonlinear dynamic progressive collapse analysis of multi-storey steel composite frame buildings — Parametric study. Engineering Structures 2010; 32(12), pp. 3974–3980.

[49] Guo, L., Liu, Y., Fu, F., Huang, H. Behavior of axially loaded circular stainless steel tube confined concrete stub columns, Thin-Walled Structures, 2019, 139, pp. 66–76

[50] Xiao Y, Kunnath S, Li FW, Zhao YB, Lew HS, Bao Y. Kunnath SK. Collapse test of three-story half-scale reinforced concrete frame building. ACI Struct J 2015; 112(4): 429-438.

[51] Yu J, Gan YP, Ji J. Behavior and design of reinforced concrete frames retrofitted with steel bracing against progressive collapse. Struct Design Tall Spec Build 2020; 29(2): e1771.

[52] Fu, F. Design and Analysis of Tall and Complex Structures and Complex Structures, 2018, Butterworth-Heinemann. ISBN 978-0-08-101121-8

[53] Deng, X.-F., Liang, S.-L., Fu, F., Qian, K. Effects of High-Strength Concrete on Progressive Collapse Resistance of Reinforced Concrete Frame Journal of Structural Engineering (United States), 2020, 146(6), 04020078

[54] Yu J, Tan KH. Special detailing techniques to improve structural resistance against progressive collapse. J Struct Eng 2014; 140: 04013077.

[55] Pham A T, Tan KH. Static and dynamic responses of reinforced concrete structures under sudd en column removal scenario subjected to distributed loading. J Struct Eng 2019; 145 (1): 04018235.

[56] Izzuddin BA, Vlassis AG, Elghazouli AY, Nethercot DA. Progressive collapse of multi-storey

buildings due to sudden column loss—Part I: Simplified assessment framework. Eng Struct 2008; 30(5):1309-18.

TABLES AND FIGURES

List of Tables:

List of Figures:

Fig. 14 Horizontal movement of the joints at different stories of BF1

Fig. 15 Resistance comparison of the frame between the corner column failure and the middle column failure

Fig. 16 The ratio of load redistribution when the middle column failure: (a) SF1; (b) SWF1

Fig. 17 The ratio of load redistribution when the corner column failure: (a) SF1; (b) SWF1

Fig. 18 Dynamic performance of models

Fig. 19 Layout of infill wall with different opening ratios: (a) 21%; (b) 32%; (c) 42%; (d) 53%

Fig. 20 Effects of opening ratio of external wall on structural resistance

Fig. 21 The first peak load capacity of infilled frame with different opening ratios

Fig. 22 Effects of story number on the first peak load capacity of structure

Fig. 23 Effects of thickness of infilled wall on structural resistance

Fig. 24 Effects of compressive strength of infilled walls on structural resistance

Table 1-Reinforcements properties

Specimen	Items	d (mm)	f_y (MPa)	f_u (MPa)	δ /%
WF&WF-L	T10	10	515	594	16.9
	R6	6	449	537	13.3
	R3	3	417	479	9.7
T1&S1	T16	16	529	608	14.3
	T13	13	535	611	11.6
	T10	10	437	568	13.1
	R6	6	355	465	17.5

Note: d, f_y, f_u and δ mean nominal diameter, yield strength, ultimate strength and elongation of reinforcement, respectively.

Table 2-Summary of simulated results

Model ID	Model Description	Critical Load (kN)		Critical Displacement (mm)		K
		F_{FPL}	F_T	u_{FPL}	u_T	($\times 10^3$ kN /m)
BF1	Bare frame	4596	4100	85	716	267
SF1	Bare frame with slab	5923	4956	88	650	360
WF1	Infilled frame	6881	4595	27	712	665
SWF1	Infilled frame with slab	7812	5361	29	648	717

Note: F_{FPL}, F_T, u_{FPL} and u_T mean first peak load capacity, ultimate load capacity from tensile catenary and their corresponding displacements, respectively; K means initial stiffness.

Table 3-Equivalent strut width and calculated results under different thicknesses of infill wall

t_{inf} (mm)	Equivalent strut widths (mm)			F_{FPL} (kN)	K (×10³ kN /m)
	a_1	a_2	a_3		
0.4 t_{inf}	553	694	488	6179	484
0.6 t_{inf}	531	666	469	6715	565
0.8 t_{inf}	516	647	456	7274	643
1.0 t_{inf}	504	633	446	7812	717
1.2 t_{inf}	495	622	438	8414	795

Note: f_m means compressive strength of infill wall; a_1, a_2, a_3 are the equivalent diagonal strut widths corresponding to the area (width × height) of 3650mm×2800mm, 5450mm×2750mm and 2150mm×2750mm, respectively

Table 4-Equivalent strut width and calculated results under different compressive strength of masonry units

f_m (MPa)	Equivalent strut widths (mm)			F_{FPL} (kN)	K (×10³ kN /m)
	a_1	a_2	a_3		
0.25 f_m	580	727	512	6004	421
0.5 f_m	541	679	478	6438	525
0.75 f_m	519	652	459	7129	624
1.0 f_m	504	633	446	7812	717
1.25 f_m	493	619	436	8554	814

Note: f_m means compressive strength of infill wall; a_1, a_2, a_3 are the equivalent diagonal strut widths corresponding to the area (width × height) of 3650mm×2800mm, 5450mm×2750mm and 2150mm×2750mm, respectively

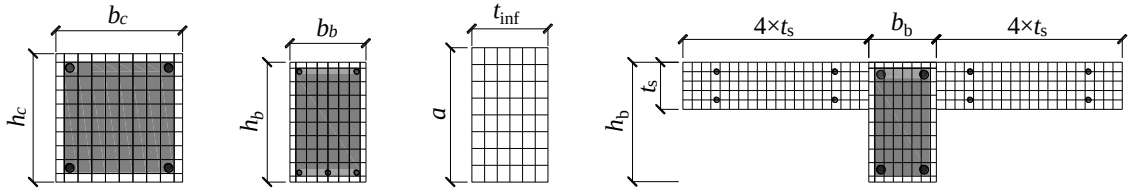

Fig. 1 Fiber division of various sections

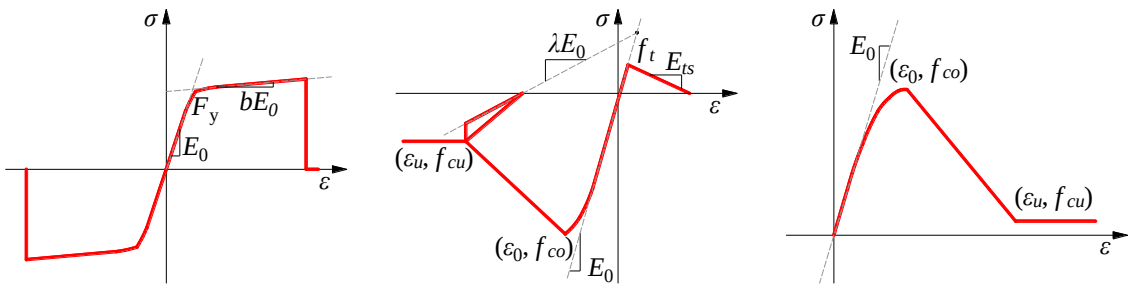

(a) Rebar (b) Concerte (c) Equivalent truss

Fig. 2 Constitutive relationship of materials

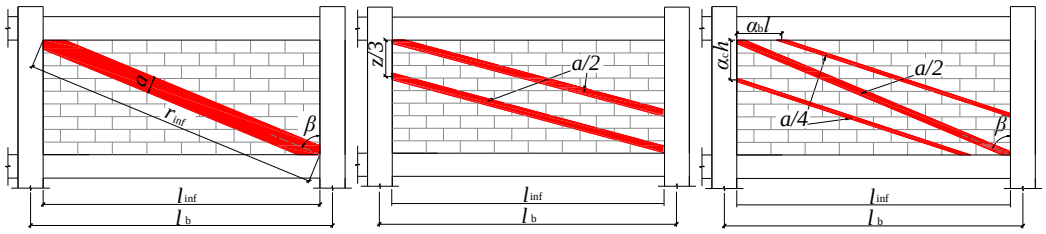

(a) (b) (c)

Fig. 3 Equivalent model for full-height infill walls: (a) single-strut model; (b) double-strut model; (c) triple-strut model

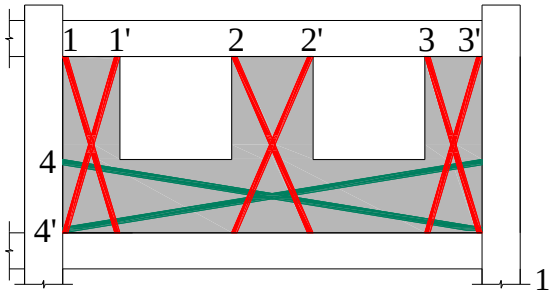

Fig. 4 Infill wall with openings represented by equivalent struts

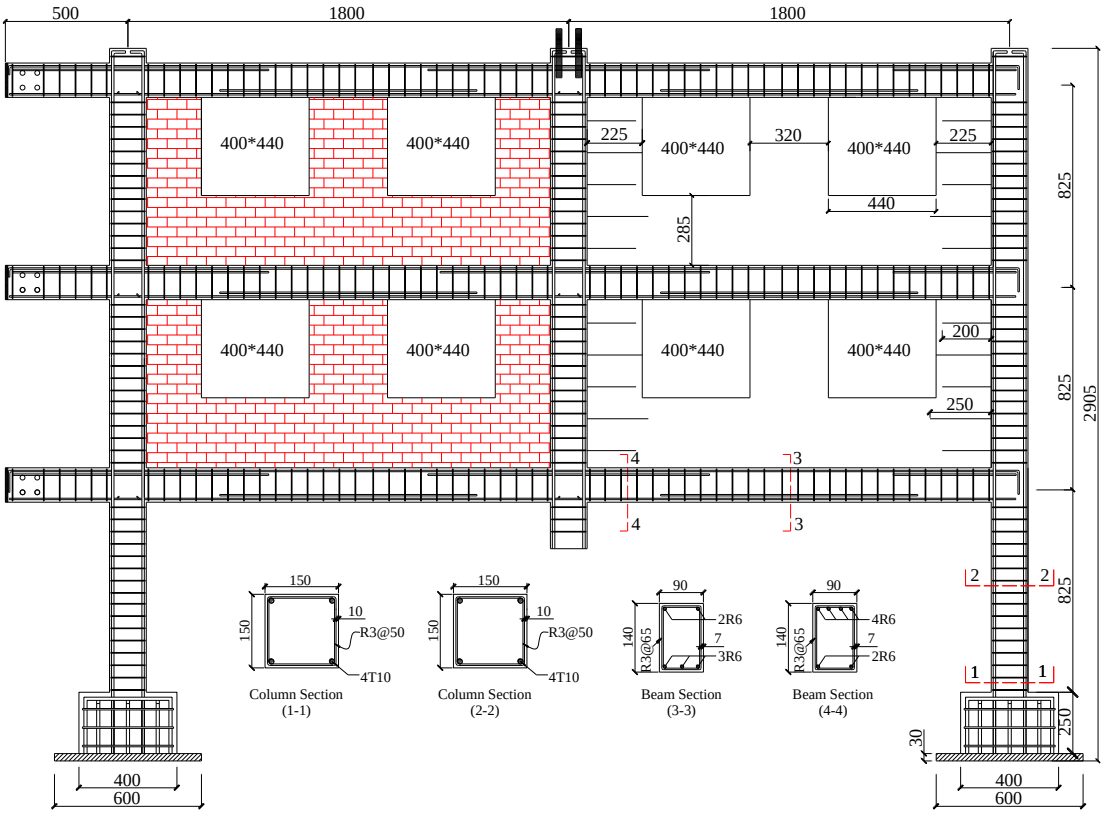

Fig. 5 Dimension and reinforcement details of Specimen WF-L (unit: mm)

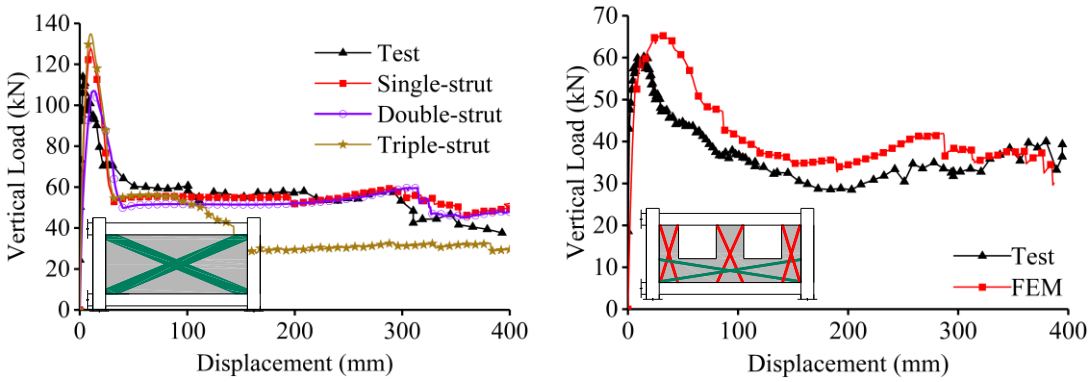

(a) (b)

Fig. 6 Comparison of tested and simulated load-displacement curve: (a)WF; (b)WF-L

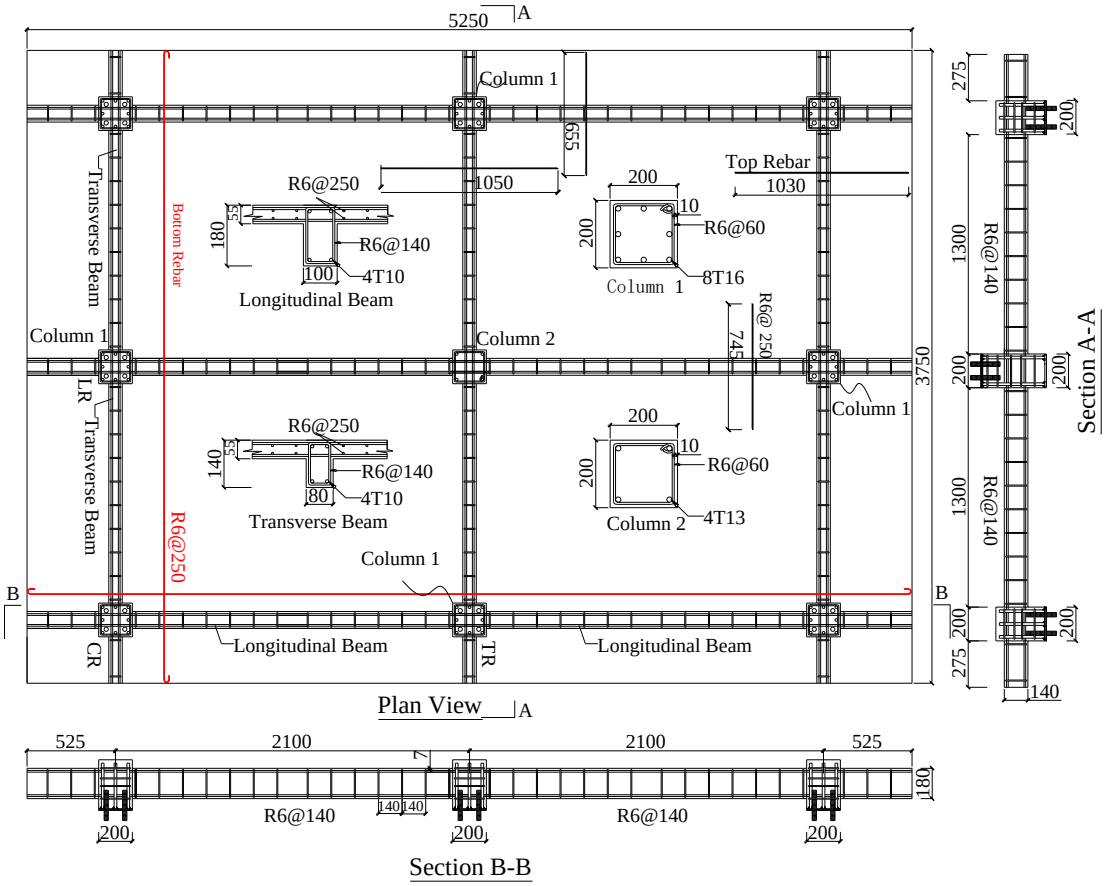

Fig. 7 Dimension and reinforcement details of Specimen S1 (unit: mm)

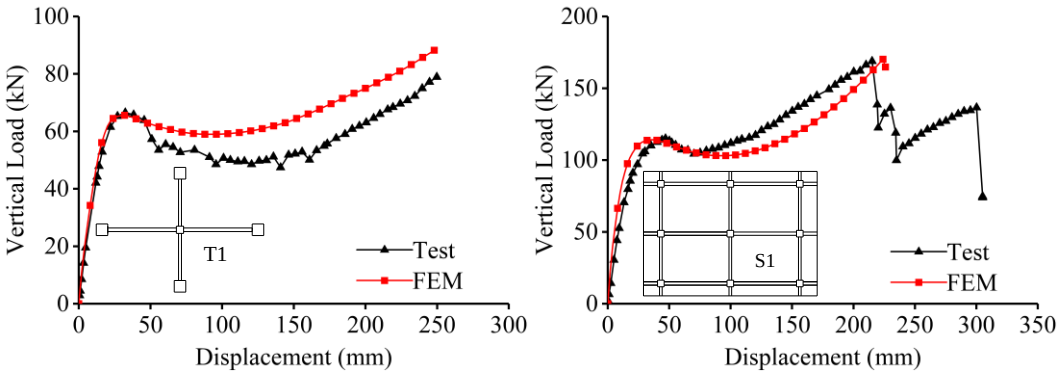

(a) (b)

Fig. 8 Comparison of tested and simulated load-displacement curve: (a)T1; (b)S1

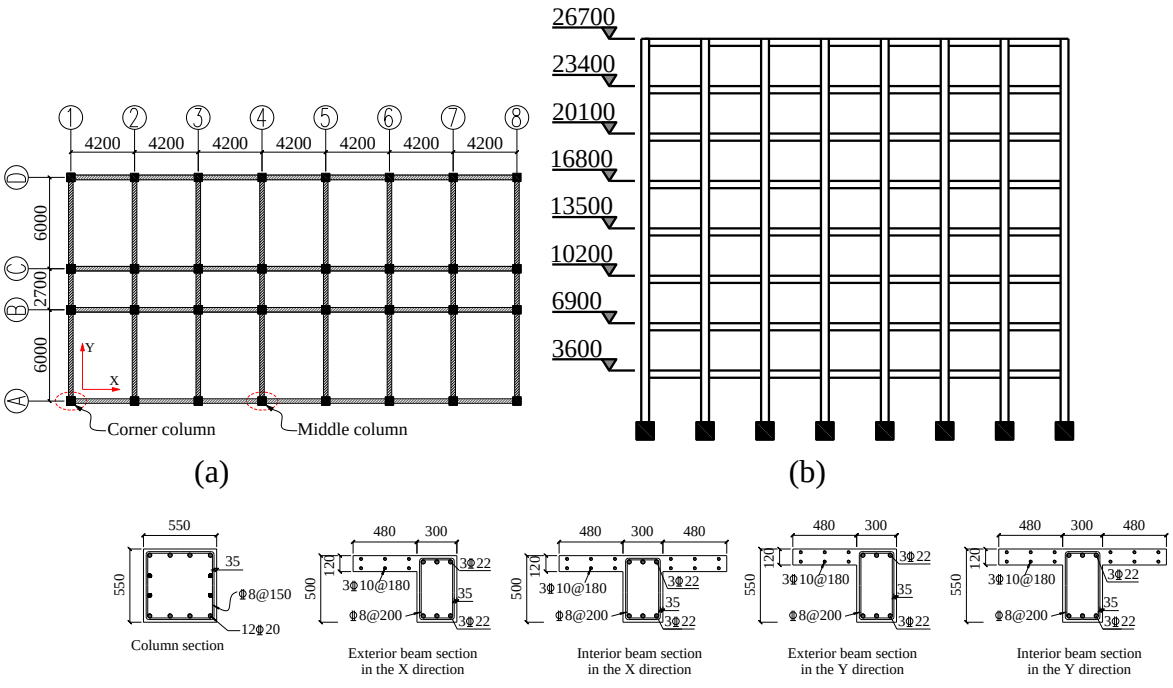

(a) (b)

(c)

Fig. 9 Geometric dimensions and cross-sectional detailing of frame: (a) plan view, (b) elevation view, (c) cross section of RC frame (unit: mm)

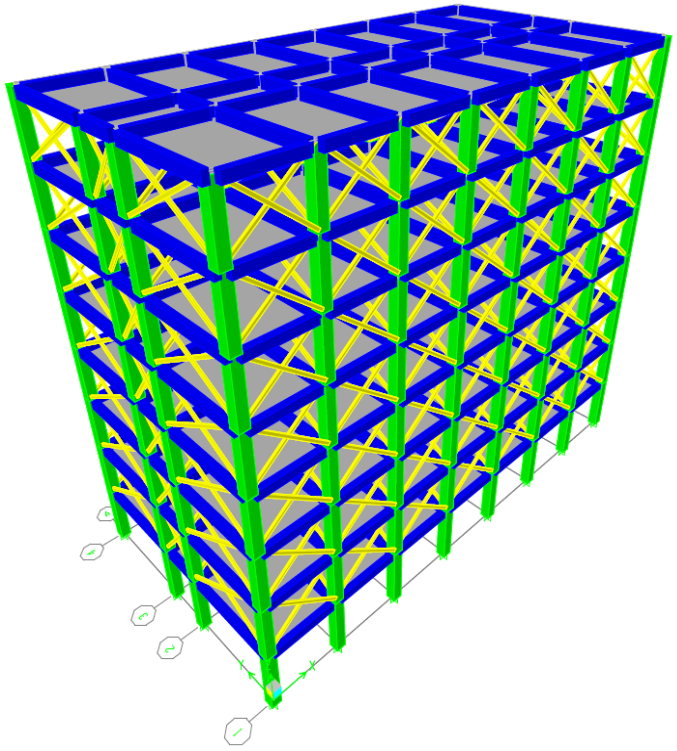

Fig. 10 General view of the model of 8-story RC infilled frame

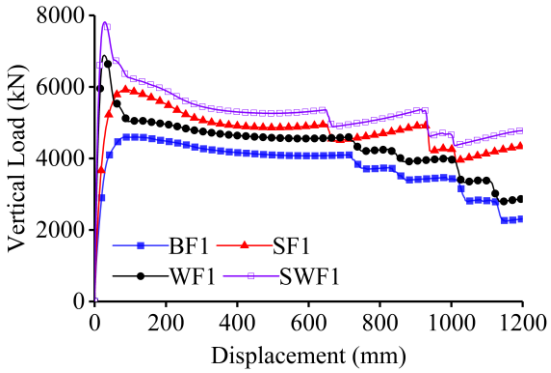

Fig. 11 Comparison of load-displacement curve of different model

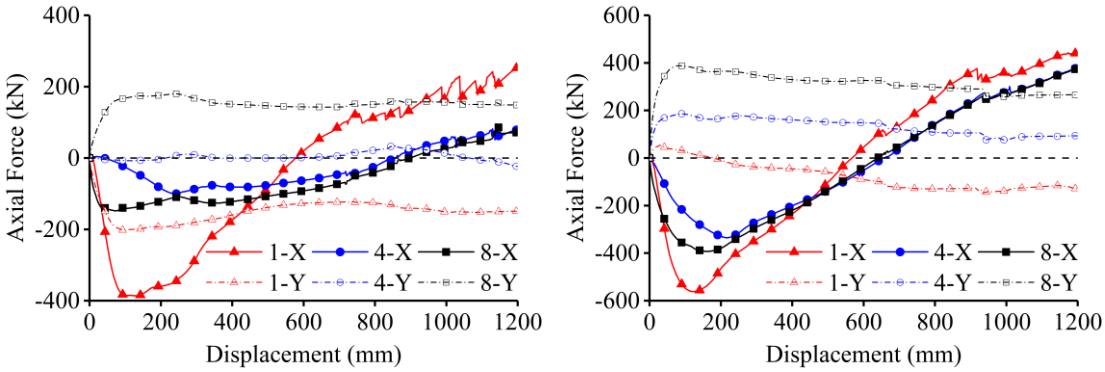

(a) (b)

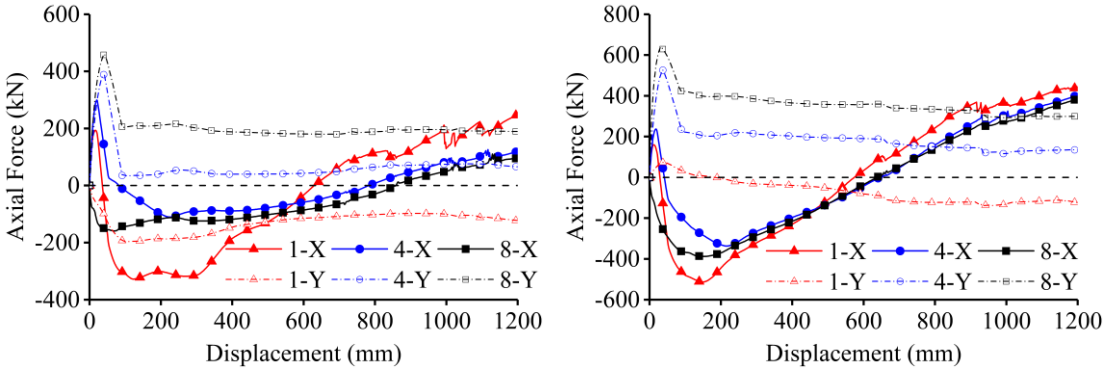

(c) (d)

Fig. 12 Axial force of beams in each layer above the failed column: (a) BF1; (b)SF1; (c) WF1; (d) SWF1

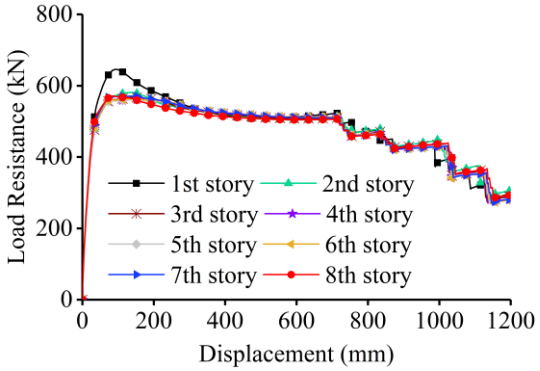

(a)

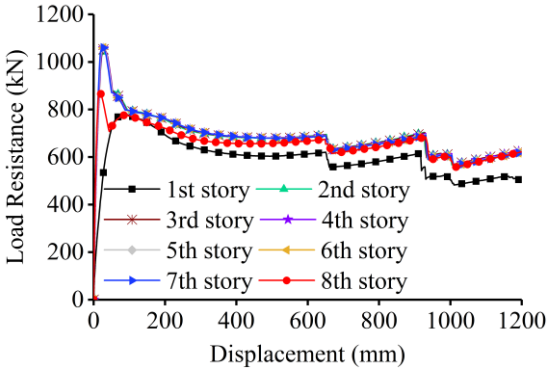

(b)

Fig. 13 Load resistance of each story: (a) BF1; (b) SWF1

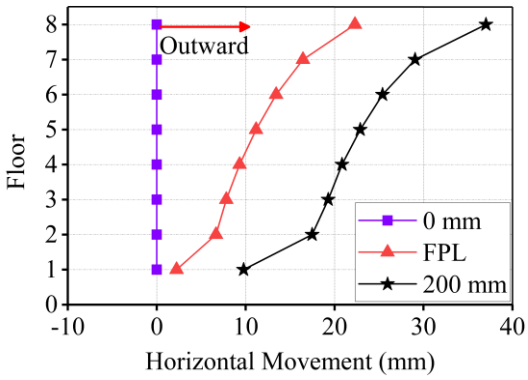

Fig. 14 Horizontal movement of the joints at different stories of BF1

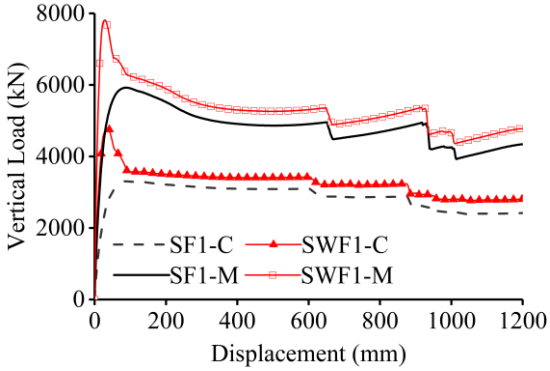

Fig. 15 Resistance comparison of the frame between the corner column failure and the middle column failure

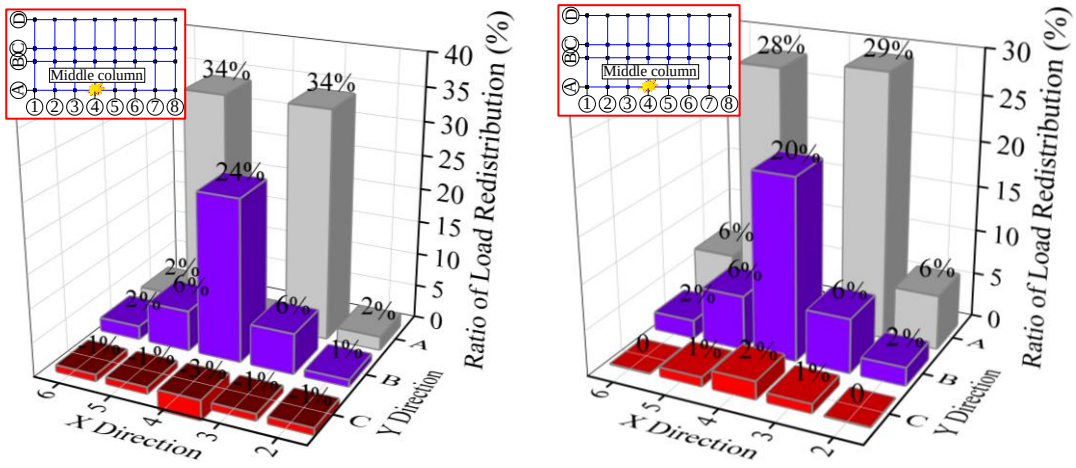

(a) (b)

Fig. 16 The ratio of load redistribution when the middle column failure: (a) SF1; (b) SWF1

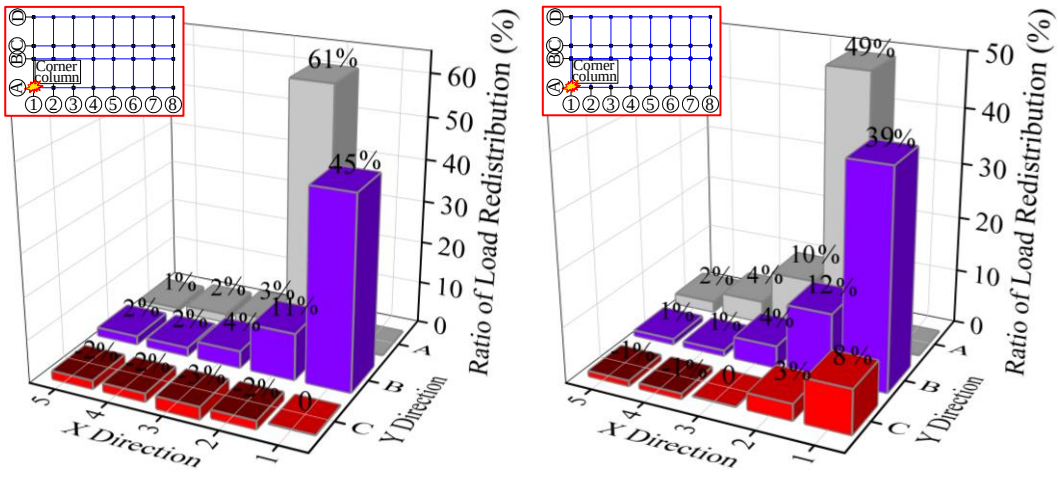

(a) (b)

Fig. 17 The ratio of load redistribution when the corner column failure: (a) SF1; (b) SWF1

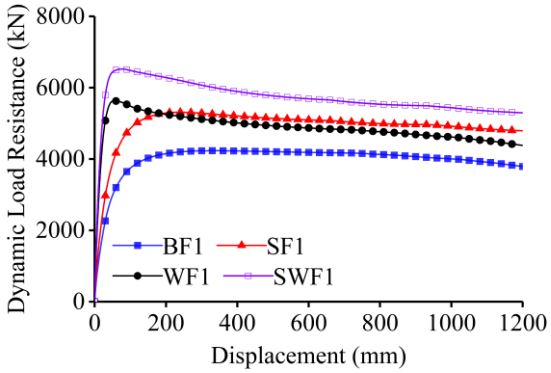

Fig. 18 Dynamic performance of models

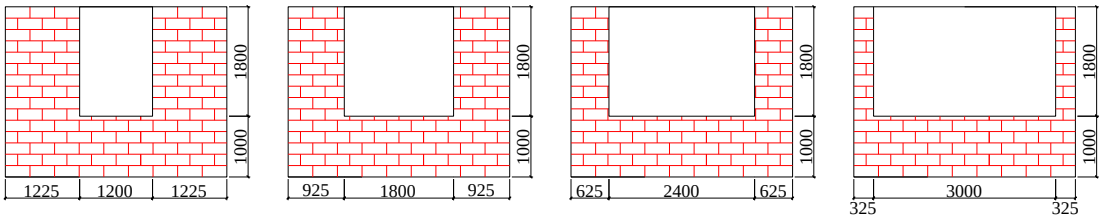

Fig. 19 Layout of infill wall with different opening ratios: (a) 21%; (b) 32%; (c) 42%; (d) 53%

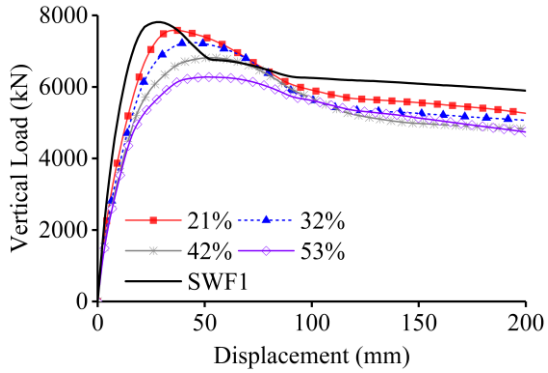

Fig. 20 Effects of opening ratio of external wall on structural resistance

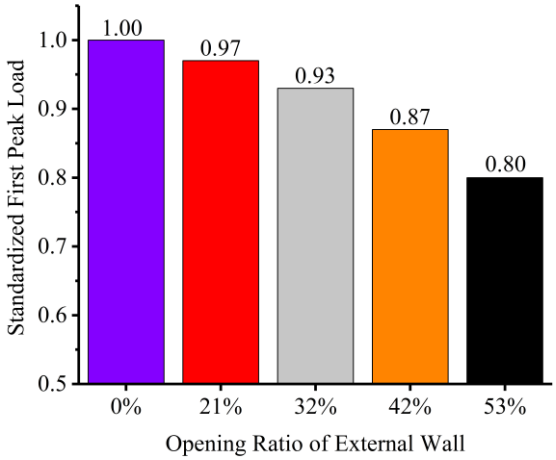

Fig. 21 The first peak load capacity of infilled frame with different opening ratios

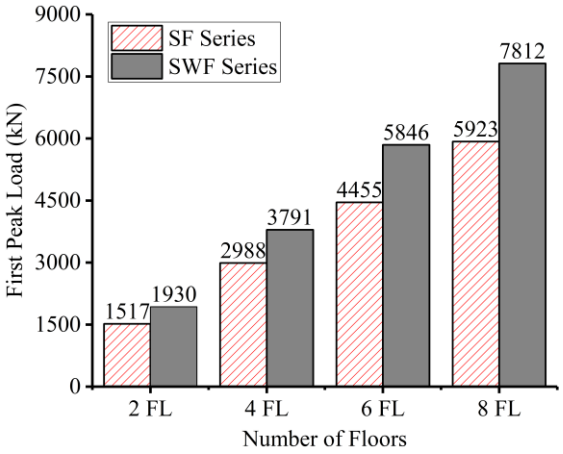

Fig. 22 Effects of story number on the first peak load capacity of structure

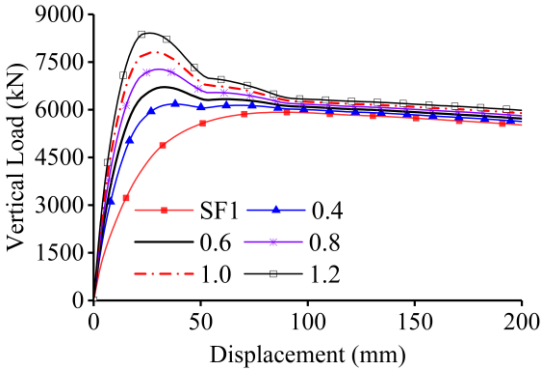

Fig. 23 Effects of thickness of infilled wall on structural resistance

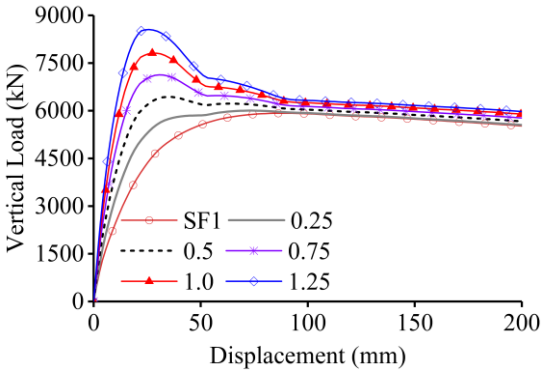

Fig. 24 Effects of compressive strength of infilled walls on structural resistance